

Wide energy range cross section of elastic electron scattering in matter: dependence of dynamical screening of target atoms on electron velocity

N. Medvedev^{1,2,*}, D.I. Zainutdinov³, A.E. Volkov³

1. Institute of Physics, Czech Academy of Sciences, Na Slovance 1999/2, 182 21 Prague 8, Czechia

2. Institute of Plasma Physics, Czech Academy of Sciences, Za Slovankou 1782/3, 182 00 Prague 8, Czechia

3. P.N. Lebedev Physical Institute of the Russian Academy of Sciences, Leninskij pr., 53, 119991 Moscow, Russia

Abstract

We present a model of electron-atoms (elastic) scattering of electrons in matter, applicable in a wide electron energy range from \sim eV up to relativistic ones. The approach based on the dynamic-structure factor considers dynamical screening of atomic nuclei in a target by valence (collective) and core-shell electrons, dependent on the incident electron velocity. The model allows simulating electron transport in matter with a unified approach to the elastic scattering. The cross section recovers the limiting cases of the electron-phonon scattering in the low energy limit, and a screened-ion scattering with the decreasing screening reducing to the scattering on a bare nucleus in the high energy limit.

I. Introduction

Radiation transport in matter is a mature field of research with a variety of applications from radiation safety, to space missions and medical treatment [1–4]. High-energy charged particles irradiation of materials is used in nanotechnologies (e.g., nanodots and nanosized channels productions) and for material properties modification [5,6]. Electron irradiation is widely used in electron diffraction and microscopy [7]. X- and γ -ray irradiation is used at synchrotrons and free-electron lasers for studying structural and dynamical processes in matter and chemical reactions [8]. Swift-heavy ion irradiation induces electron cascades along the ion trajectories followed by spatial spreading of the generated electrons, which leads to energy deposition to target atoms causing finally formation of observable and latent ion tracks [9,10].

In these irradiation scenarios, electron transport plays a crucial role [9,11]. At typical energies of incident particles, triggering an electron cascade, the electrons have energies from \sim MeV down to \sim eV energies and lower. A high energy electron experiences three main channels of interaction with matter [9,11–15]: (i) scattering on target electrons, exciting electrons from core atomic shells or valence/conduction band (impact ionization or excitation of collective electronic modes – plasmons), called *inelastic scattering*; (ii) scattering transferring energy to the

* Email: nikita.medvedev@fzu.cz

target atoms (including excitation of their collective modes – phonons) without electron ionization, referred to as *elastic scattering*; (iii) photon emission *via* Bremsstrahlung process, which is important only at high relativistic energies.

Transport Monte Carlo (MC) simulations is the standard technic for modeling of electron transport and accompanying effects [9,12,16,17]. The scattering cross sections of projectiles are the key parameters of these simulations. They describe the scattering probabilities of a particle, its mean free path, and energy loss in a target [9,11,14,15,18]. The inelastic electron scattering cross sections, accounting for collective response of the material, were studied in the previous works, see e.g. [19–24]. Here, we will focus on the elastic scattering channel defined above.

Simulations of elastic scattering of an electron in matter usually rely on a patchwork of approximations: low-energy electrons are assumed to scatter on collective atomic oscillations – phonons, whereas high-energy electrons interaction is assumed to be with individual and dynamically independent atoms [11,13–15]. The intermediate region, where neither of these approximations work (typically for electron energies in the range from a few eV up to a hundred eV), is not covered well with existing models. Thus, we propose a model based on the dynamic-structure factor formalism, naturally unifying these limiting cases and covering a wide range of electron energies.

II. Model

1. General form of elastic scattering cross section

To derive a general form of the elastic scattering of an electron on a coupled system of nuclei and electrons forming a material of interest, we start with the first-order Born approximation, which assumes plane waves for an incident particle [25–27]. The double differential cross section of interaction of an electron is expressed as follows:

$$\frac{d^2\sigma}{d(\hbar q)d(\hbar\omega)} = \frac{q}{2\pi\hbar^3 v^2} \sum_{i,f} P_i |\langle f | \langle k_f^e | \hat{V}_{int} | k_i^e \rangle | i \rangle|^2 \delta(\hbar\omega - (E_f - E_i)). \quad (1)$$

Here $\hbar\omega$ is the transferred energy, $\hbar q$ is the transferred momentum (wave vector), with \hbar being the Planck constant; v is the incident electron velocity; E_f and E_i are, correspondingly, its final and initial energies; $|i\rangle$ and $|f\rangle$ are the initial and the final states of the target; $|k_{i,f}^e\rangle$ are the initial and final states of the incident electron, \hat{V}_{int} is the interaction potential; the scattering matrix element is averaged over the initial target states with the factors P_i (Gibbs or Boltzmann statistical weights of the medium states in thermal equilibrium) [25–27]. Here, an isotropic and uniform target medium is assumed.

The pairwise Coulomb interaction of the electron with charged particles in the target (nuclei and electrons) is:

$$\hat{V}_{int} = - \sum_{j=1}^{N_i} \frac{Ze^2}{(\mathbf{r} - \mathbf{R}_j)} + \sum_{j=1}^{N_e} \frac{e^2}{(\mathbf{r} - \mathbf{r}_j)}, \quad (2)$$

here R_j and r_j are the coordinates of the nuclei and electrons, respectively; the nuclei have the charge Ze (e is the electron charge); the terms are summed over all nuclei N_i and electrons N_e of the target.

In the plane waves approximation for the incident and scattered electronic states ($|k_{i,f}^e\rangle = V^{-\frac{1}{2}} \exp(i\mathbf{k}_{i,f}^e \cdot \mathbf{r})$, with V being the volume of the scattering system, the cross section then splits into the following sum [28]:

$$\frac{d^2\sigma}{d(\hbar q)d(\hbar\omega)} = \frac{q}{2\pi\hbar^4} \frac{1}{v^2} \left(\frac{4\pi e^2}{q^2} \right)^2 (S_{ee}(\omega, q) - ZS_{ei}(\omega, q) - ZS_{ie}(\omega, q) + Z^2S_{ii}(\omega, q)), \quad (3)$$

where the partial dynamic structure factors are defined as [25–27]:

$$S_{ab}(q, \omega) = \sum_i P_i \left\langle i \left| \int \frac{dt}{2\pi} \exp(i\omega t) \int d\mathbf{r} \int d\mathbf{r}' \exp(-i\mathbf{q}(\mathbf{r} - \mathbf{r}')) \hat{n}_a(\mathbf{r}, t) \hat{n}_b(\mathbf{r}', 0) \right| i \right\rangle, \quad (4)$$

the indices {a,b} mark electrons (e) and ions(i), and the number-density operators are $\hat{n}_e(\mathbf{r}, t) = \sum_{l=1}^{N_e} \delta(\mathbf{r} - \hat{\mathbf{r}}_l^e(t))$ and $\hat{n}_i(\mathbf{r}, t) = \sum_{l=1}^{N_a} \delta(\mathbf{r} - \hat{\mathbf{R}}_l^i(t))$.

Following the idea of Chihara's decomposition [29], we split the electronic contributions $S_{ie}(q, \omega)$, $S_{ei}(q, \omega)$ and $S_{ee}(q, \omega)$ into the core-shells and the 'free' electrons (belonging to the valence or the conduction band of the material). The core-shell electrons are assumed to follow their parenting ions adiabatically, whereas valence/conduction electrons are free particles influenced by the potential of ions.

In this case, the cross section of the electron scattering can be separated into two parts describing its scattering on the atomic and electronic systems of a target. The elastic scattering cross section on the atomic ensemble can then be rewritten as follows with the screened nucleus charge:

$$\frac{d^2\sigma_{e-at}}{d(\hbar q)d(\hbar\omega)} = \frac{q}{2\pi\hbar^4} \frac{1}{v^2} \left(\frac{4\pi e^2}{q^2} \right)^2 (Z - Z_I f_I(\tilde{q}) - \rho(\omega, \tilde{q}))^2 S_{ii}(\omega, q). \quad (5)$$

Here $Z - Z_I f_I(\tilde{q}) - \rho(\omega, \tilde{q})$ is the charge of an atom that scatters the electron, $f_I(\tilde{q})$ is the atomic form-factor build up by core-shell electrons only without the 'free' valence electrons, $Z_I = Z - N_{VB}$; N_{VB} is the number of valence electrons per atom or element of a compound; $\rho(\tilde{q}, \omega)$ is the electron cloud of the 'free' electrons around the ion core [29].

We assume that both quantities, defining the induced charge *via* the screening of the nucleus by the electrons, respond to some common momentum in the system of the target and the incident electron, \tilde{q} , which will be discussed below. In the original Chihara's paper [29], this momentum is equal to the transferred one $\tilde{q} = q$, since that work only considered scattering of

incident photons which are moving with the speed of light. Here, incident electrons are considered which carry charge and travel at different velocities below the speed of light. The nucleus screening depends on the velocity of the incident electron: the faster the electron – the less screened nuclei it “feels”, without the contribution of target/atomic electrons having velocities smaller than that of the incident one.

2. Model of atomic loss function

The ion-ion (or atomic) dynamic structure factor, entering Eq.(5), may be calculated with the classical molecular-dynamics simulations [30,31]. Alternatively, the fluctuation-dissipation theorem can be used that in thermal equilibrium links the dynamical structure factor of an ensemble of charged particles with its loss function – the imaginary part of the inverse complex dielectric function [32]:

$$Im \left[-\frac{1}{\varepsilon(\omega, q)} \right] = \frac{4\pi e^2}{q^2 \hbar} \left(1 - e^{-\frac{\hbar\omega}{T}} \right) S(\omega, q). \quad (6)$$

For a target consisting of atoms and electrons, Eq. (6) transforms to the following:

$$Im \left[-\frac{1}{\varepsilon(\omega, q)} \right] = \frac{4\pi e^2}{q^2 \hbar} \left(1 - e^{-\frac{\hbar\omega}{T}} \right) (S_{ee}(\omega, q) - ZS_{ei}(\omega, q) - ZS_{ie}(\omega, q) + Z^2 S_{ii}(\omega, q)), \quad (7)$$

where the approximation from Eq. (5) allows us to obtain the atomic (phonon) part of the loss function:

$$Im \left[-\frac{1}{\varepsilon_{at}(\omega, q)} \right] = \frac{4\pi e^2}{q^2 \hbar} \left(1 - e^{-\frac{\hbar\omega}{T}} \right) (Z - Z_I f_I(\tilde{q}) - \rho(\omega, \tilde{q}))^2 S_{ii}(\omega, q). \quad (8)$$

The loss function of a solid can be reconstructed from the experimental optical data on the low-energy photon scattering [33,34] whose cross section is proportional to the DSF of the atomic system of a solid [29]:

$$\left(\frac{d^2 \sigma}{d(\hbar q) d(\hbar \omega)} \right)_{at,exp}^{opt} \sim Im \left[\frac{-1}{\varepsilon_{at,exp}^{opt}(\omega, q)} \right] = \frac{4\pi e^2}{q^2 \hbar} \left(1 - e^{-\frac{\hbar\omega}{T}} \right) Z_{opt}^2 S_{ii}(\omega, q), \quad (9)$$

where the screened charge of atoms in Eq. (9) can be considered constant in the low-energy limit (denoted Z_{opt}).

However, the target's reaction to low-energy photon irradiation does not include the dependence of atomic charges on the photon momentum (required in Eq. (8)), or information on acoustic phonons. This results in a difference between the experimental loss function obtained from the optical data $Im \left[\frac{-1}{\varepsilon_{at,exp}^{opt}(\omega, q)} \right]$ and the partial loss function $Im \left[-\frac{1}{\varepsilon_{at}(\omega, q)} \right]$ describing the scattering of an electron on the atomic ensemble of a target. It is similar to the atomic form factors restored from photon, electron or neutron scattering: they are different being restored from the cross sections of different scattering channels (see, e.g., the Mott–Bethe formula connecting the atomic form factors of electron and photon scattering [35,36]).

As a result, the effective charge of an atom involved in the photon absorption Z_{opt} differs from that for the scattering of electrons $Z_{e-at} = (Z - f_I(\tilde{q}) - \rho(\tilde{q}))$. Z_{opt} can be calculated from the f -sum-rule for the experimental optical loss function [23]:

$$Z_{opt}^2 = \frac{2}{\pi \hbar^2 \Omega_p^2} \int_0^\infty Im \left[\frac{-1}{\varepsilon_{at,exp}^{opt}(\omega, q)} \right] (\hbar\omega) d(\hbar\omega), \quad (10)$$

where $\Omega_p^2 = 4\pi e^2 \sum_i n_i / M_i$, n_i is density of atoms of the i -th type in the compound, and M_i are their masses (for example, in Al_2O_3 $Z_{opt} \approx 0.81$, and in SiO_2 $Z_{opt} \approx 0.86$).

Comparing Eqs.(8) and (9), we obtain the connection between the calculated loss function for electron-atom (electron-phonon) scattering and the one reconstructed from the optical data:

$$Im \left[\frac{-1}{\varepsilon_{at}(\omega, q)} \right] = \frac{(Z - f_I(\tilde{q}) - \rho(\tilde{q}))^2}{Z_{opt}^2} Im \left[\frac{-1}{\varepsilon_{at,exp}^{opt}(\omega, q)} \right]. \quad (11)$$

Eqs.(10-11) enable rewriting the cross section of scattering of electrons on the atomic ensemble of a target (Eq.(5)) *via* the loss function reconstructed from the optical data:

$$\begin{aligned} \frac{d^2 \sigma_{e-at}}{d(\hbar q) d(\hbar \omega)} &= \frac{2e^2}{n_i \pi \hbar^2 v^2} \frac{1}{\hbar q} \left(1 - e^{\frac{\hbar \omega}{k_B T}} \right)^{-1} \times \\ &\frac{(Z - f_I(\tilde{q}) - \rho(\omega, \tilde{q}))^2}{Z_{opt}^2} Im \left[\frac{-1}{\varepsilon_{at,exp}^{opt}(\omega, q)} \right]. \end{aligned} \quad (12)$$

Denoting the renormalized loss function as $Im \left[\frac{-1}{\tilde{\varepsilon}_{at}(\omega, q)} \right] = \frac{1}{Z_{opt}^2} Im \left[\frac{-1}{\varepsilon_{at,exp}^{opt}(\omega, q)} \right]$, the electron elastic scattering cross-section turns into:

$$\frac{d^2 \sigma_{e-at}}{d(\hbar q) d(\hbar \omega)} = \frac{2e^2}{n_i \pi \hbar^2 v^2} \frac{1}{\hbar q} \left(1 - e^{\frac{\hbar \omega}{k_B T}} \right)^{-1} (Z - f_I(\tilde{q}) - \rho(\omega, \tilde{q}))^2 Im \left[\frac{-1}{\tilde{\varepsilon}_{at}(\omega, q)} \right]. \quad (13)$$

The induced charge associated with the electronic cloud of 'free' electrons may be expressed *via* the valence-band part of the complex dielectric function (CDF) [37]:

$$\rho(\omega, \tilde{q}) = N_{VB} \left(1 - \frac{1}{|\varepsilon_{VB}(\omega, \tilde{q})|} \right), \quad (14)$$

producing the final expression for the electron elastic scattering in a material:

$$\begin{aligned} \frac{d^2 \sigma_{e-at}}{d(\hbar q) d(\hbar \omega)} &= \frac{2e^2}{n_i \pi \hbar^2 v^2} \frac{1}{\hbar q} \left(1 - e^{\frac{\hbar \omega}{k_B T}} \right)^{-1} \\ &\times \left[Z - Z_I f_I(\tilde{q}) - N_{VB} \left(1 - \frac{1}{|\varepsilon_{VB}(\omega, \tilde{q})|} \right) \right]^2 Im \left[\frac{-1}{\tilde{\varepsilon}_{at}(\omega, q)} \right]. \end{aligned} \quad (15)$$

The atomic form factors for neutral atoms are available in the literature [12,38], however further approximation may be needed to treat the contributions of ions without the valence electrons in solids. Following the typical shapes of the form-factors of ions [39], we assume the following expression: $Z_I f_I(\tilde{q}) = \min(Z_I, Z f_a(\tilde{q}))$ (where $f_a(\tilde{q})$ is the atomic form factor of a neutral atom with the same atomic number Z). Here we use the form factors from Ref. [12].

The used practical model for the valence-band electronic complex dielectric and loss functions will be discussed in the next section.

The effective momentum defining the screening, \tilde{q} , depends on the properties of both, the incident electron as well as the target's system of the nucleus and electrons in each atomic shell. Here, we make an *ad hoc* approximation defining this quantity as follows:

$$\tilde{q} = (q + k_i^e)/2, \quad (16)$$

This approximation is chosen to account for the momenta in both fractions of the entire system of charges – the incident electron momentum (wave vector k_i^e) and the momentum transferred to the atomic system of the target, q .

We note that Eq.(15) recovers known limiting cases. For a scattering of an electron on an isolated atom ($N_{VB} = 0$, $Z_I = Z$) and $\tilde{q} = q$, the standard scattering cross section is restored [40]:

$$\frac{d^2 \sigma_{e-at}}{d(\hbar q) d(\hbar \omega)} \sim (Z - Z f_a(q))^2.$$

Note that the same limit is reached for fast particles, which interact with a solid as with an ensemble of independent ions [25].

For the case of a fully ionized plasma, ($N_{VB} = Z$, $Z_I = 0$), the standard electron-ion scattering is recovered (again, assuming $\tilde{q} = q$):

$$\frac{d^2 \sigma_{e-at}}{d(\hbar q) d(\hbar \omega)} \sim \left(\frac{Z}{\varepsilon(\omega, q)} \right)^2.$$

3. Model of screening by valence-band electrons

It is, in principle, possible to calculate the valence-band complex dielectric function of a multicomponent system, entering Eq.(15), with *ab initio* methods, such as density-functional based Kubo-Greenwood approach or more advanced techniques [41,42]. However, for practical applications, e.g. in MC simulations, a convenient analytical model of the valence-band complex dielectric function is required. We propose to use the formalism developed by Ritchie and Howie to reconstruct the electronic loss function from the optical coefficients in the form of a sum of Drude-Lorentz-type oscillators [23]. When $q=0$ (in the optical limit), it can be approximated as follows:

$$Im \left[\frac{-1}{\varepsilon_{VB}(\omega, q=0)} \right] = \sum_{i=1}^{N^{os}} \frac{A_i \gamma_i \hbar \omega}{[\hbar^2 \omega^2 - E_{0i}^2(q=0)]^2 + (\gamma_i \hbar \omega)^2}, \quad (17)$$

here N^{os} oscillators are used to reproduce the valence band part of the loss function from experimental data on the optical complex refractive index (see the detailed algorithm description, e.g., in [22,43]); E_{0i} describes the positions of the maximum of i -th oscillator, γ_i is the oscillator width (loosely associated with the electronic relaxation time), and A_i is i -th oscillator weight, defining contribution of i -th oscillator into the total loss function and constrained by the sum rules [22,43]. If the optical data are unavailable for the material of interest, further approximations for the coefficients may be made, allowing to approximately evaluate the loss function [34].

The analytical extension into the finite $q>0$ values is then done *via* the replacement $E_{0i}(q) \rightarrow E_{0i}(q=0) + \hbar^2 q^2 / (2m)$, where m is the mass of the scattering centre (the electron mass m_e in $\varepsilon_{VB}(\omega, q)$ or the target atom mass in $\varepsilon_{ph}(\omega, q)$) [22,44].

Having the loss function, the real part of the inverse CDF may be restored in the analytical form using Kramers-Kronig relations:

$$Re \left[\frac{-1}{\varepsilon_{VB}(\omega, q)} \right] = - \left(1 - \sum_{i=1}^{N^{os}} \frac{A_i (E_{0i}^2(q) - (\hbar \omega)^2)}{[\hbar^2 \omega^2 - E_{0i}^2(q)]^2 + (\gamma_i \hbar \omega)^2} \right), \quad (18)$$

and the complex dielectric function is then recovered:

$$Re[\varepsilon_{VB}(\omega, q)] = - \frac{Re \left[\frac{-1}{\varepsilon_{VB}(\omega, q)} \right]}{Re \left[\frac{-1}{\varepsilon_{VB}(\omega, q)} \right]^2 + Im \left[\frac{-1}{\varepsilon_{VB}(\omega, q)} \right]^2}, \quad (19)$$

$$Im[\varepsilon_{VB}(\omega, q)] = \frac{Im \left[\frac{-1}{\varepsilon_{VB}(\omega, q)} \right]}{Re \left[\frac{-1}{\varepsilon_{VB}(\omega, q)} \right]^2 + Im \left[\frac{-1}{\varepsilon_{VB}(\omega, q)} \right]^2}.$$

Note that in the case of a single oscillator $N^{os} = 1$, the CDF reduces to a simpler analytical expression of the Drude-like oscillator:

$$\varepsilon_{VB}(\omega, q) = 1 + \frac{A_1}{E_{01}^2(q) - A_1 - (\hbar \omega)^2 - i \gamma_1 \hbar \omega}. \quad (20)$$

Eqs. (19) or (20) can be used to evaluate the contribution to the screening by the valence-band electrons in Eq.(15).

III. Results

The above-described formalism was implemented in TREKIS-3 code [45]. It enables us to evaluate the electron elastic mean free paths in a variety of materials. For those materials, for which the phonon CDF coefficients are unknown (such as metals and Si), the single-pole approximation is used with coefficients approximated from the characteristic phonon frequency and the sum rules [34].

For comparison, we will also use here the approximation proposed for dielectric compounds in [33] (and used in our earlier papers [21,44,46]) where the screened charge in Eq.(13) was replaced by:

$$\left(Z - Z_I f_I(\tilde{q}) - N_{VB} \left(1 - \frac{1}{|\epsilon_{VB}(\omega, \tilde{q})|} \right) \right) \rightarrow 1, \quad (21)$$

and $Im \left[\frac{-1}{\tilde{\epsilon}_{at}(\omega, q)} \right] \rightarrow Im \left[\frac{-1}{\tilde{\epsilon}_{at,exp}^{opt}(\omega, q)} \right]$. In this case, electrons scatter on atoms with the "effective" charge corresponding to the loss function extracted from scattering of low-energy photons. Below, such calculations will be marked as "Z=1".

Alternatively, we proposed to describe the effective charge of a target atom by a formula similar to the Barkas one developed for the effective charge of an incident ion in matter [34]:

$$\left(Z - Z_I f_I(\tilde{q}) - N_{VB} \left(1 - \frac{1}{|\epsilon_{VB}(\omega, \tilde{q})|} \right) \right) \rightarrow$$

$$Z_B = 1 + (Z - 1) \left\{ 1 - \exp \left[-\frac{v}{v_0} (Z - 1)^{-\frac{2}{3}} \right] \right\} \quad (22)$$

where v is the incident electron velocity, and $v_0=c/125$ is empirically adjusted atomic electron velocity [47]. This adjustment was constructed to reproduce the case $Z=1$ at low electron energies but reduce the screening to the scattering on a bare nucleus at high electron energies. Calculation with this effective charge will be marked in the plots as "Barkas-like". This expression reduces to $Z=1$ at the low-energy limit independently of the material and may overestimate the scattering cross section at the intermediate electron energies (see below).

We also compare our results with the often-used screened Rutherford cross section with modified Molier screening parameter (marked in the plots below as "R-M") [14].

The calculated electron elastic mean free paths (MFP) in a few materials are presented below. We start by discussing a few elemental solids and then move to compounds.

In silicon, shown in Figure 1, the calculated data are compared with the few other calculations from the literature. At low energies, the calculation agree reasonably well with the electron-phonon calculations from [48] and [49]. At high energies, the cross section (and, correspondingly, the mean free path) reproduces the nuclear charge with the reducing screening *via* Barkas-like empirical formula from [34]. At energies above some 10 keV, both reduce to the scattering on unscreened nuclear charge. In this high energy limit, the scattering is reasonably

close to the scattering on an isolated atom, which is reproduced with the adjusted R-M, and to the NIST database [50].

Thus, we can conclude that the derived Eq.(15) with the used parameters for the phononic and valence band of the loss function reproduces reasonably well both limiting cases, at low energy (electron phonon scattering) and at high energies (electron scattering on an individual ion, close to NIST data and R-M cross section). In contrast, the approximations of $Z=1$ and Barkas-like expression fail to reproduce the low- and intermediate energy limit; this is the reason why atomic cross sections are often replaced with the electron-phonon scattering cross sections at low energies in MC simulations.

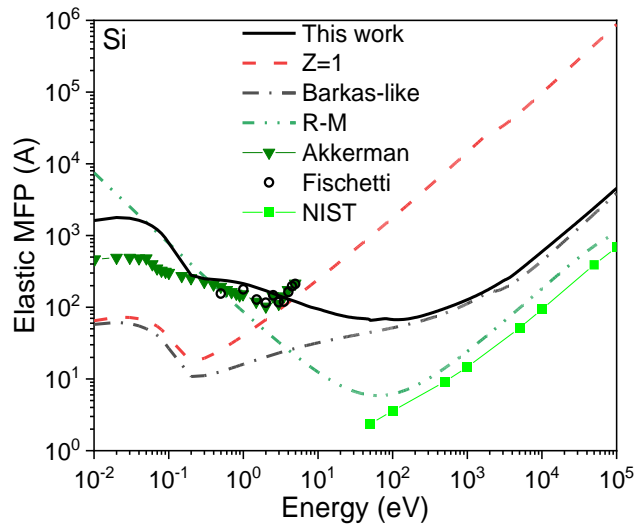


Figure 1. Elastic mean free path of electron scattering in silicon, calculated with Eq.(15) and compared with other approximations: the calculated electron-phonon scattering from Akkerman and Murat *et al.* [48], Fischetti and Laux [49], and electron-atomic scattering at high energies from NIST database [50].

Figure 2 shows the calculated elastic MFP in aluminum, where again, the high-energy limit is reasonably close to the R-M cross section, NIST database [50], and phase-shift calculations by Dapor *et al.* [51]. At lower energies, the full-screening expression (Eq.(15)) predicts noticeably larger mean free paths, in contrast to $Z=1$ and Barkas-like approximations that produce MFPs that strike us as unrealistically short. Unfortunately, there are no experimental data to compare with.

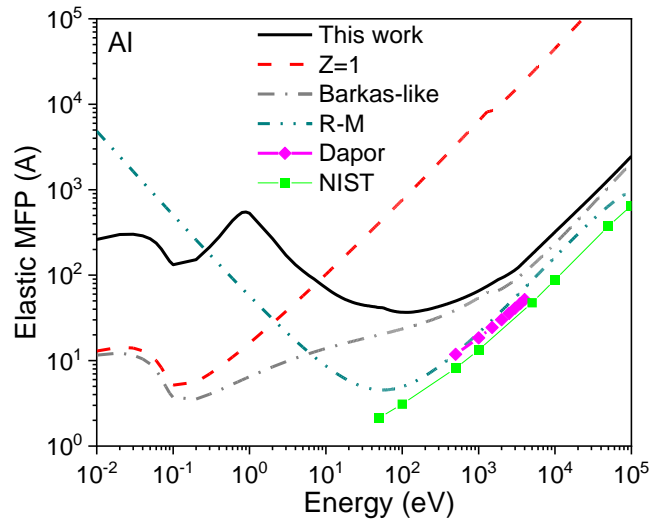


Figure 2. Elastic mean free path of electron scattering in aluminum, calculated with Eq.(15), compared with other approximations, and the calculated electron-atomic scattering at high energies by Dapor [51], and from NIST database [50].

Figure 3 shows the calculated elastic MFP in gold, where again, the high-energy limit is reasonably close to the R-M cross section, NIST database [50], and phase-shift calculations by Dapor *et al.* [51]. We note that in this case, our calculations agree with NIST database and Dapor’s results even better than R-M cross section.

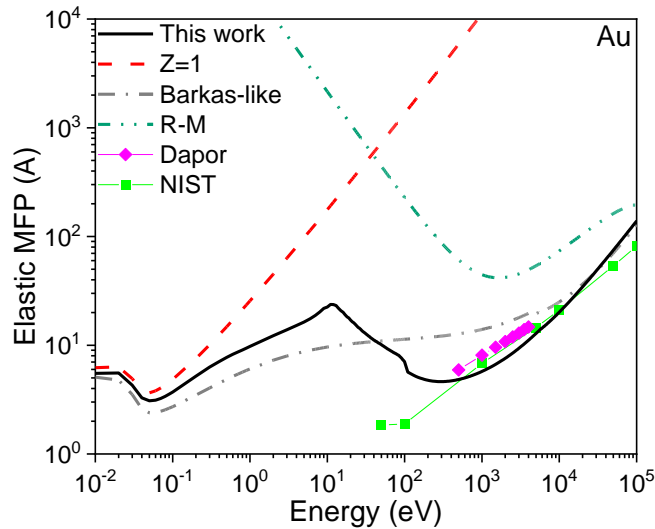


Figure 3. Elastic mean free path of electron scattering in gold, calculated with Eq.(15), compared with other approximations, and the calculated electron-atomic scattering at high energies by Dapor [51], and from NIST database [50].

Figure 4 shows the calculated elastic MFP in SiC. As in the materials above, the high-energy limit is reasonably close to the R-M cross section. In this case, the R-M cross section was constructed for the compound using the additivity rule [52]. In contrast to such atomic calculations, the methodology of Eq.(15) does not rely on the additivity rule, but describes the collective behavior (structure and dynamics) of the solid *via* the dynamic structure factor and the complex dielectric functions.

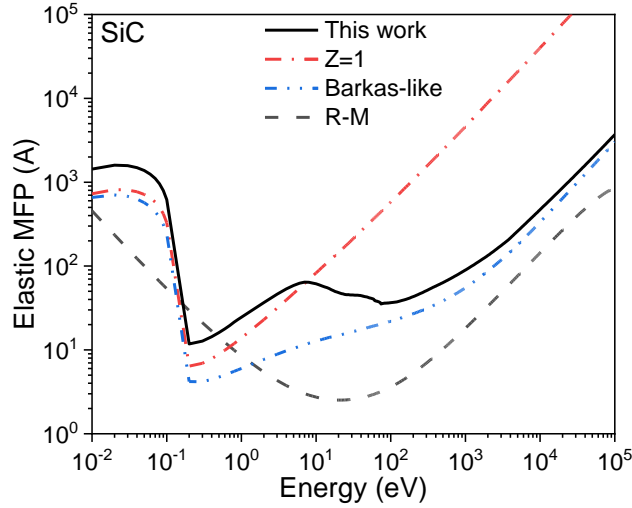


Figure 4. Elastic mean free path of electron scattering in SiC, calculated with Eq.(15), compared with other approximations.

Figure 5 shows the calculated elastic MFP in SiO₂. At low energies, we also compare our results with calculations by Kuhr and Fitting [33], which used CDF-based formalism similar to ours with Z=1 approximation – which, thus, resembles this limiting case. Their more recent version of MC modeling used scattering of electrons on optical and acoustic phonons in SiO₂ (in Figure 5 added via the Matthiessen rule), which shows an even closer agreement with our calculations [53]. Calculations by Fischetti et al. are also close to those at low energies, but have a much deeper drop at electron energies above ~3 eV [54]. Our calculated high-energy limit coincides with the Barkas-like approximation, and is reasonably close to the R-M cross sections with additivity rule, which almost coincides with Dapor’s atomic calculations [55]. Considering the differences among various models in the literature, our agreement with the limiting cases seems reasonable.

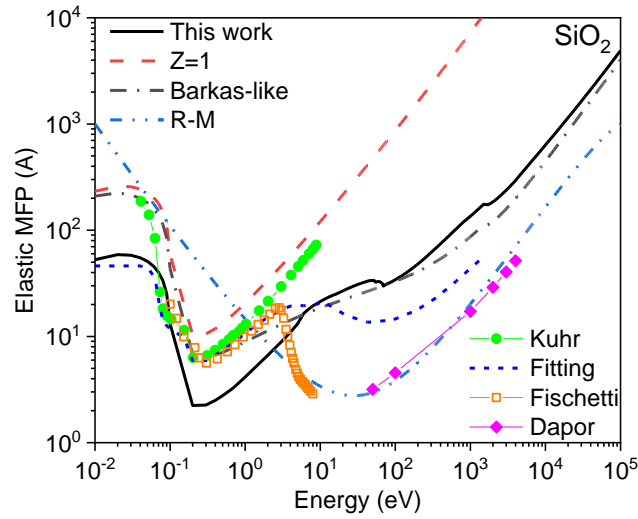


Figure 5. Elastic mean free path of electron scattering in SiO_2 , calculated with Eq.(15), compared with other approximations by Kuhr and Fitting [33], Fitting et al. [53], Fischetti et al. [54]; and Dapor's calculations [55].

Figure 6 shows the calculated elastic MFP in Al_2O_3 , where again, the high-energy limit coincides with the Barkas-like approximation and is reasonably close to the R-M cross sections with additivity rule. At low energies, the calculated MFPs are close to those from Barkas and Z=1 approximations.

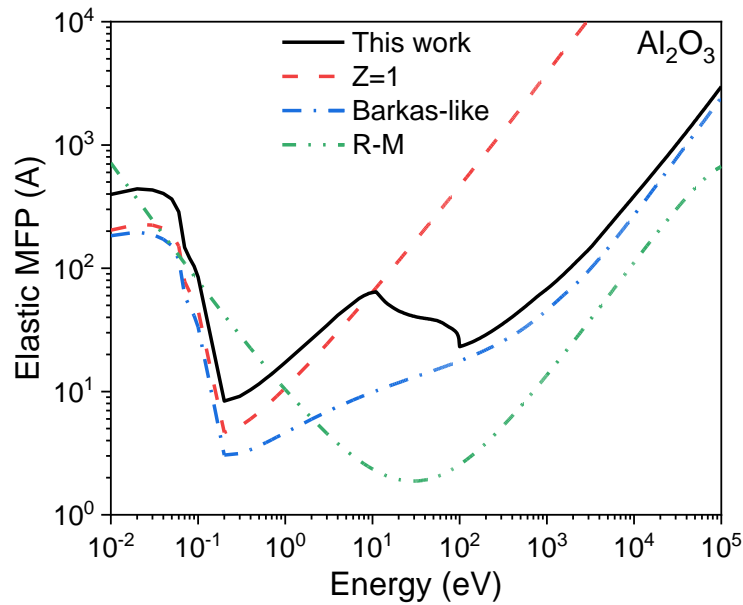


Figure 6. Elastic mean free path of electron scattering in Al_2O_3 , calculated with Eq.(15), compared with other approximations.

Summarizing, we conclude that the proposed model of electron elastic scattering in matter describes a wide range of energies in a satisfactory agreement with both limiting cases: electron-phonon scattering at low energies and scattering on an individual atom at high energies. Such a unified model absolves the user from seeking a patchwork of different approximations, allowing for more consistent modeling. It may be implemented, e.g., in standard Monte Carlo simulations and compared with experimental data on energy transport after material irradiation, which will be a topic of a future dedicated research.

IV. Conclusions

A new model of evaluation of the cross section of electron scattering on the atomic system (elastic scattering) in matter is proposed. It is based on the dynamic structure factor (linear response theory) formalism. The developed cross section unifies the limiting cases of the electron-phonon scattering in the low-energy limit, and electron-ion scattering similar to scattering on the atomic gas in the high-energy one. Comparison with the available simulations shows a reasonable agreement in both limits in various materials. The formalism enables straightforward implementation, e.g., in Monte Carlo simulations, avoiding a patchwork of low-energy and high-energy-limit approximations.

V. Acknowledgements

The authors thank F. Akhmetov for valuable discussions. NM thanks the financial support from the Czech Ministry of Education, Youth, and Sports (grants No. LTT17015, LM2023068, and No. EF16_013/0001552), and the computational resources supplied by the project "e-Infrastruktura CZ" (e-INFRA LM2018140) provided within the program Projects of Large Research, Development and Innovations Infrastructures. DIZ's work has been carried out using computing resources of the federal collective usage center Complex for Simulation and Data Processing for Mega-science Facilities at NRC "Kurchatov Institute", <http://ckp.nrcki.ru/>.

VI. Code and data availability

The code TREKIS-3 used to obtain the results presented in this study is available from [45].

VII. References

- [1] R. Fleischer, H. Hart, and W. Giard, *Particle Track Identification: Application of a New Technique to Apollo Helmets*, *Science* **170**, 1189 (1970).
- [2] K. Masumura, K. Kuniya, T. Kurobe, M. Fukuoka, F. Yatagai, and T. Nohmi, *Heavy-Ion-*

- Induced Mutations in Thegpt Delta Transgenic Mouse: Comparison of Mutation Spectra Induced by Heavy-Ion, X-Ray, and γ -Ray Radiation*, Environ. Mol. Mutagen. **40**, 207 (2002).
- [3] F. A. Cucinotta and M. Durante, *Cancer Risk from Exposure to Galactic Cosmic Rays: Implications for Space Exploration by Human Beings*, Lancet. Oncol. **7**, 431 (2006).
- [4] T. L. Phillips, R. (Richard) Hoppe, M. Roach, and S. A. Leibel, *Leibel and Phillips Textbook of Radiation Oncology* (Elsevier/Saunders, 2010).
- [5] E. Akcöltekin, T. Peters, R. Meyer, A. Duvenbeck, M. Klusmann, I. Monnet, H. Lebius, and M. Schleberger, *Creation of Multiple Nanodots by Single Ions*, Nat. Nanotechnol. **2**, 290 (2007).
- [6] S. Dutt, P. Apel, N. Lizunov, C. Notthoff, Q. Wen, C. Trautmann, P. Mota-Santiago, N. Kirby, and P. Kluth, *Shape of Nanopores in Track-Etched Polycarbonate Membranes*, J. Memb. Sci. **638**, 119681 (2021).
- [7] G. A. de la Peña Muñoz et al., *Ultrafast Lattice Disordering Can Be Accelerated by Electronic Collisional Forces*, Nat. Phys. 2023 1 (2023).
- [8] J. Rossbach, J. R. Schneider, and W. Wurth, *10 Years of Pioneering X-Ray Science at the Free-Electron Laser FLASH at DESY*, Phys. Rep. **808**, 1 (2019).
- [9] N. Medvedev, A. E. Volkov, R. Rymzhanov, F. Akhmetov, S. Gorbunov, R. Voronkov, and P. Babaev, *Frontiers, Challenges, and Solutions in Modeling of Swift Heavy Ion Effects in Materials*, J. Appl. Phys. **133**, 100701 (2023).
- [10] F. F. Komarov, *Nano- and Microstructuring of Solids by Swift Heavy Ions*, Physics-Uspekhi **60**, 435 (2017).
- [11] M. Dapor, *Electron Transport in Solids*, Springer Tracts Mod. Phys. **271**, 1 (2020).
- [12] F. Salvat and M. Fern, *PENELOPE-2014 – A Code System for Monte Carlo Simulation of Electron and Photon Transport*, 2015th ed. (NUCLEAR ENERGY AGENCY, Organisation for Economic Co-operation and Development, Barcelona, Spain, 2015).
- [13] A. F. Akkerman, *Modeling of Charged Particles Trajectories in Matter* (Nauka, Moscow, 1991).
- [14] T. M. Jenkins, W. R. Nelson, and A. Rindi, *Monte Carlo Transport of Electrons and Photons* (Springer US, Boston, MA, 1988).
- [15] C. Jacoboni and L. Reggiani, *The Monte Carlo Method for the Solution of Charge Transport in Semiconductors with Applications to Covalent Materials*, Rev. Mod. Phys. **55**, 645 (1983).
- [16] X-5 Monte Carlo Team, *MCNP – A General Monte Carlo N-Particle Transport Code, Version 5 Volume 1: Overview and Theory*, Revised 10, Vol. 1 (Los Alamos National Laboratory, University of California, 2003).
- [17] A. Ferrari, P. R. Sala, A. Fassò, and J. Ranft, *Fluka: A Multi-Particle Transport Code*: [Http://Www.Fluka.Org/Content/Manuals/FM.Pdf](http://www.fluka.org/content/manuals/fm.pdf), 2005.
- [18] T. Apostolova et al., *Tools for Investigating Electronic Excitation: Experiment and Multi-Scale Modelling* (Universidad Politécnica de Madrid. Instituto de Fusión Nuclear Guillermo Velarde, Madrid, 2021).

- [19] N. Medvedev and A. E. Volkov, *Analytically Solvable Model of Scattering of Relativistic Charged Particles in Solids*, J. Phys. D: Appl. Phys. **53**, 235302 (2020).
- [20] N. Medvedev and A. E. Volkov, *Corrigendum: Analytically Solvable Model of Scattering of Relativistic Charged Particles in Solids (2020 J. Phys. D: Appl. Phys. 53 235302)*, J. Phys. D: Appl. Phys. **55**, 019501 (2021).
- [21] N. A. Medvedev, R. A. Rymzhanov, and A. E. Volkov, *Time-Resolved Electron Kinetics in Swift Heavy Ion Irradiated Solids*, J. Phys. D: Appl. Phys. **48**, 355303 (2015).
- [22] A. Akkerman, T. Boutboul, A. Breskin, R. Chechik, A. Gibrekhterman, and Y. Lifshitz, *Inelastic Electron Interactions in the Energy Range 50 eV to 10 keV in Insulators: Alkali Halides and Metal Oxides*, Phys. Status Solidi Basic Res. **198**, 769 (1996).
- [23] R. H. Ritchie and A. Howie, *Electron Excitation and the Optical Potential in Electron Microscopy*, Philos. Mag. **36**, 463 (1977).
- [24] R. Garcia-Molina, I. Abril, I. Kyriakou, and D. Emfietzoglou, *Inelastic Scattering and Energy Loss of Swift Electron Beams in Biologically Relevant Materials*, Surf. Interface Anal. **49**, 11 (2017).
- [25] L. Van Hove, *Correlations in Space and Time and Born Approximation Scattering in Systems of Interacting Particles*, Phys. Rev. **95**, 249 (1954).
- [26] K. Sturm, *Dynamic Structure Factor: An Introduction*, Zeitschrift Für Naturforsch. A **48**, 233 (1993).
- [27] V. T. Shvets, *Multi-Particle Dynamic Structure Factors for a Noninteracting Electron Gas*, Theor. Math. Phys. **106**, 359 (1996).
- [28] V. T. Shvets and A. P. Fedtchuk, *Electron-Phonon Interaction and Electronic Transport Phenomena in Amorphous Transition Metals*, Phys. Scr. **52**, 722 (1995).
- [29] J. Chihara, *Interaction of Photons with Plasmas and Liquid Metals - Photoabsorption and Scattering*, J. Phys. Condens. Matter **12**, 231 (2000).
- [30] S. A. Gorbunov, A. E. Volkov, and R. A. Voronkov, *Periodic Boundary Conditions Effects on Atomic Dynamics Analysis*, Comput. Phys. Commun. **279**, 108454 (2022).
- [31] S. A. Gorbunov, P. N. Terekhin, N. A. Medvedev, and A. E. Volkov, *Combined Model of the Material Excitation and Relaxation in Swift Heavy Ion Tracks*, Nucl. Instruments Methods Phys. Res. Sect. B Beam Interact. with Mater. Atoms **315**, 173 (2013).
- [32] C. Kittel, *Quantum Theory of Solids* (1963).
- [33] J.-C. Kuhr and H.-J. Fitting, *Monte Carlo Simulation of Electron Emission from Solids*, J. Electron Spectros. Relat. Phenomena **105**, 257 (1999).
- [34] N. Medvedev, F. Akhmetov, R. A. Rymzhanov, R. Voronkov, and A. E. Volkov, *Modeling Time-Resolved Kinetics in Solids Induced by Extreme Electronic Excitation*, Adv. Theory Simulations **5**, 2200091 (2022).
- [35] *The Scattering of Electrons by Atoms*, Proc. R. Soc. London. Ser. A, Contain. Pap. a Math. Phys. Character **127**, 658 (1930).

- [36] H. Bethe, *Zur Theorie Des Durchgangs Schneller Korpuskularstrahlen Durch Materie*, Ann. Phys. **397**, 325 (1930).
- [37] N. H. March and M. P. Tosi, *Atomic Dynamics in Liquids* (Courier Corporation, Chelmsford, 1991).
- [38] D. E. Cullen, EPICS2017: Electron Photon Interaction Cross Sections: W-Nds.Iaea.Org/Epics/, 2018.
- [39] S. P. Hau-Riege, *X-Ray Atomic Scattering Factors of Low-Z Ions with a Core Hole*, Phys. Rev. A **76**, 042511 (2007).
- [40] L. D. Landau and L. M. Lifshitz, *Quantum Mechanics, Third Edition: Non-Relativistic Theory*, 3 edition, (Butterworth-Heinemann;, 1976).
- [41] B. Holst, V. Recoules, S. Mazevet, M. Torrent, A. Ng, Z. Chen, S. E. Kirkwood, V. Sametoglu, M. Reid, and Y. Y. Tsui, *Ab Initio Model of Optical Properties of Two-Temperature Warm Dense Matter*, Phys. Rev. B - Condens. Matter Mater. Phys. **90**, 35121 (2014).
- [42] L. Calderín, V. V. Karasiev, and S. B. Trickey, *Kubo–Greenwood Electrical Conductivity Formulation and Implementation for Projector Augmented Wave Datasets*, Comput. Phys. Commun. **221**, 118 (2017).
- [43] N. Medvedev, *Modeling Ultrafast Electronic Processes in Solids Excited by Femtosecond VUV-XUV Laser Pulse*, AIP Conf. Proc. **582**, 582 (2012).
- [44] R. A. Rymzhanov, N. A. Medvedev, and A. E. Volkov, *Effects of Model Approximations for Electron, Hole, and Photon Transport in Swift Heavy Ion Tracks*, Nucl. Instruments Methods Phys. Res. Sect. B Beam Interact. with Mater. Atoms **388**, 41 (2016).
- [45] N. Medvedev, R. Rymzhanov, and A. Volkov, *TREKIS-3 [Computer Software]*, <https://doi.org/10.5281/zenodo.8394462>.
- [46] R. Rymzhanov, N. A. Medvedev, and A. E. Volkov, *Damage Threshold and Structure of Swift Heavy Ion Tracks in Al₂O₃*, J. Phys. D: Appl. Phys. **50**, 475301 (2017).
- [47] W. H. Barkas, *Nuclear Research Emulsions*. (Academic Press, New York, 1963).
- [48] A. Akkerman and M. Murat, *Electron–Phonon Interactions in Silicon: Mean Free Paths, Related Distributions and Transport Characteristics*, Nucl. Instruments Methods Phys. Res. Sect. B Beam Interact. with Mater. Atoms **350**, 49 (2015).
- [49] M. V. Fischetti and S. E. Laux, *Monte Carlo Study of Electron Transport in Silicon Inversion Layers*, Phys. Rev. B **48**, 2244 (1993).
- [50] A. Jablonski, F. Salvat, C. J. Powell, and A. . Y. Lee, *NIST Electron Elastic-Scattering Cross-Section Database*, <https://srdata.nist.gov/SRD64/Elastic>.
- [51] M. Dapor and A. Miotello, *Differential, Total, and Transport Cross Sections for Elastic Scattering of Low Energy Positrons by Neutral Atoms (Z= 1–92, E= 500–4000 EV)*, At. Data Nucl. Data Tables **69**, 1 (1998).
- [52] D. I. Thwaites, *Bragg’s Rule of Stopping Power Additivity: A Compilation and Summary of Results*, Radiat. Res. **95**, 495 (1983).

- [53] H.-J. Fitting, E. Schreiber, J.-C. Kuhr, and A. von Czarnowski, *Attenuation and Escape Depths of Low-Energy Electron Emission*, J. Electron Spectros. Relat. Phenomena **119**, 35 (2001).
- [54] M. V. Fischetti, D. J. DiMaria, S. D. Brorson, T. N. Theis, and J. R. Kirtley, *Theory of High-Field Electron Transport in Silicon Dioxide*, Phys. Rev. B **31**, 8124 (1985).
- [55] M. Dapor, *A Comparative Study of Electron and Positron Penetration in Silicon Dioxide*, J. Electron Spectros. Relat. Phenomena **151**, 182 (2006).